Effect of oxygen content and charge on the structure, stability and optoelectronic properties of yttrium oxide clusters

ARTICLE *in* JOURNAL OF PHYSICS AND CHEMISTRY OF SOLIDS · JULY 2015

Impact Factor: 1.85 · DOI: 10.1016/j.jpcs.2015.03.001

1 AUTHOR:

Venkataramanan Natarajan Sathiyamoorthy

SASTRA University

41 PUBLICATIONS **811** CITATIONS

SEE PROFILE

Journal of Physics and Chemistry of Solids 82 (2015) 91–100

Contents lists available at ScienceDirect

Journal of Physics and Chemistry of Solids

journal homepage: www.elsevier.com/locate/jpcs

Effect of oxygen content and charge on the structure, stability and optoelectronic properties of yttrium oxide clusters

Natarajan Sathiyamoorthy Venkataramanan *

Department of Chemistry, School of Chemical and Biotechnology, SASTRA University, Thanjavur 631401, India

ARTICLE INFO

Article history:
Received 10 October 2014
Received in revised form
31 December 2014
Accepted 2 March 2015
Available online 3 March 2015

Keywords:
Optical materials
Oxides
Ab initio calculations
Electronic structure
Optical properties

ABSTRACT

The electronic and geometrical structures of neutral and charged YO*n* (n=2–12) clusters have been investigated using density functional theory (DFT) with generalized gradient approximation. The oxygen atom in YO*n* has been found to be in oxo, peroxo and in superoxo forms. The geometrical structures and topologies of small size anionic clusters resemble that of neutral clusters. Yttrium showed higher coordination number than scandium. Computed results reveal the existence of YO_{10} cluster to have a penta-peroxo oxygen with a homoleptic $Y(\eta^2-O_2)_5$ geometrical configuration. The HOMO–LUMO gaps decrease with increasing n due to the increase in 2p orbital population of oxygen atoms. It has been shown that in these clusters bonding are predominantly ionic in nature and anions are thermodynamically more stable, due to the charge delocalization between the metal atom and oxygen ligands. YO_{10}^+ and YO_{12}^+ were found to be highly exothermic to release one and two oxygen molecules, while YO_{11}^+ dissociates though the ozonide dissociation channel. Computed absorption spectra of small clusters are mainly contributed by yttrium metal d and s valence orbitals. The absorbance spectra, shifts towards lower energy with cluster size increase, while charge has no substantial effect on the absorption spectrum.

1. Introduction

Oxides of transition metals do play an important role in various catalytic and biological processes and consequently are the subject of numerous experimental and theoretical studies [1–3]. The transition metal atom with incomplete filled d-shell were able to form diverse oxide clusters, as dioxygen can bind to the metal centers in various ways such as side-on, end-on, or split to individual atoms, leading to the formation of peroxo-, superoxo-, oxoperoxides oxosuperoxides and ozonide forms [4,5]. The coordination number of oxygen atoms is an important property of an oxide cluster, which has a close relationship with the structural compactness and bonding character. It provides a clue to understand the microstructure of bulk oxide materials by methods such as NMR. There exist many studies on first row transition metal oxides. However, only little attention has been paid to heavy transition metal oxides [6].

Yttrium oxide is the most familiar yttrium compound which is also one of the most creep resistance oxides. Furthermore, yttrium oxide is a component of ceramic materials such as yttrium aluminum garnet (YAG) finds applications in optical sensors, is used as X-ray detection material and in high temperature ceramic composites [7]. Besides the above, yttrium oxide materials have low-thermal expansion, high optical transparency, low acoustic loss, high threshold for optical damage, hardness, and general stability against chemical and mechanical interactions. The oxide a high temperature infrared (IR) and electronic material, and it has many attractive applications [8]. Moreover, yttrium oxide has been widely investigated as a host material for rare-earth ion doping, used in optical applications due to its excellent chemical stability, high optical transparency in the far-IR region and high band gap [9]. For the above pointed reasons, several studies have been carried out on the optical properties of lanthanides doped on the Y_2O_3 crystals.

The optical constants, namely the refractive index and extinction coefficient (k), of Y_2O_3 play a critical role in designing optical and electro-optic devices [10]. Specifically, significant efforts were directed to enhance the refractive index, which is expected to lead the optical transmission enhancement. However, refractive index and extinction coefficient profiles of real Y_2O_3 films are highly dependent on their microstructure [11]. Recent studies have shown that the increase in the oxygen flow during the preparation of Y_2O_3 films, results in structure transforms from cubic to polycrystalline and then to amorphous states [12]. Furthermore, the disordered structure of Y_2O_3 film facilitates the acquirement of low values of refractive index values [13]. Hence, the ability to tailor the properties and optimize performance requires a detailed

* Fax: +91 4362 264 120.
E-mail addresses: nsvenkataramanan@gmail.com, venkataramanan@scbt.sastra.edu

http://dx.doi.org/10.1016/j.jpcs.2015.03.001
0022-3697/

understanding of the relationship between electronic and geometric structure, particularly at the nanoscale level.

Among the oxides clusters of group 3 elements, scandium oxides are well studied; however little information is know about yttrium oxides [14–18]. Knickelbein probed the ionization potential (IPs) of Y*n* and Y*n*O clusters in a size range from 2 to 31 atoms [19]. Matrix isolated infrared spectroscopic studies of yttrium monoxide shows the formation of complexes with a coordination of multiple noble gas atoms [20]. Further, under oxygen rich condition, the initially formed yttrium dioxide molecule interacts spontaneously with additional O_2 molecules to form the oxygen-rich superoxo bisozonide complex [21]. A study on laser-ablated Y and La atom reactions with molecular oxygen showed the formation of metal oxides, which were absorbed on matrix [22]. The IR spectra for the matrix absorbed YO molecule showed a 12.1 cm^{-1} red-shift from the gas-phase value. In addition, Wu and Wang carried out vibrationally resolved photodetachment studies on YO*n* ($n=1$–5) clusters. The photoelectron spectra of yttrium oxide cluster anions were studied by Nakajima and coworkers [23]. The threshold energies of the photoelectron spectra were found to shift to higher binding energies with the cluster size increase. Ducan and Reed carried out a photodissociation studies on yttrium oxide cluster cations [24]. Photodissociation occurs by a sequential process, with the loss of Y_2O_3 with the predominant formation of $Y_6O_8^+$ cluster.

Xiong and Yang carried out DFT study to understand the structural, electronic and magnetic properties of yttrium clusters with oxygen atom [25]. The magnetic moments of the yttrium clusters were quenched by the introduction of oxygen atom. The introduction of dioxygen atom near the yttrium clusters showed that the oxygen molecule undergoes dissociative addition on clusters, while the O_2 absorbed structures were unstable [26]. Further, the Y_3O_2 anion was found to more stable compared to other clusters. In addition, the magnetic moment of the clusters were very small, and it is mainly due to the 4*d* and 5*s* electrons of Y atom. The low lying electronic state of YO_2^- molecules were computed by Mok and coworkers [27]. The Franck–Condon spectra computed using the coupled-cluster with single and double and petrubated triple excitations (CCSD(T)) method are in excellent agreement with the photodetachement spectrum obtained at the 355 nm excitation. In the recent DFT study made on the small yttrium trioxide clusters, it was indicated that the neutral and anion have similar geometry [28]. Among the trioxides, Y_4O_3 was found to have higher stability with zero magnetic moment, while its anion has 3 μB magnetic moment. Recently, Deshpande and coworkers carried out DFT studies on neutral and charged Y_2O_3 clusters to understand their growth pattern [29]. They observed the increase of the charge transfer from Y atom with the increase in cluster size and the clusters preference for the lowest spin state.

The oxidation number of Y is the same as that of Sc as both the elements belong to the same group three in the periodic table. As yttrium atom is bigger in size has more lanthanide character and has higher electron affinity: can yttrium atom bind more oxygen atoms than scandium? Unfortunately there are no experimental or theoretical data on the structure of YO*n* for $n>4$. The present paper is aimed at systematic search of the geometrically stable YO*n* isomers for $n=2$ to 12 using the density functional theory (DFT). Next we have performed extensive calculations to identify the effect of oxygen content on the stability and electronic properties of neutral and charged YO*n* clusters. We also computed the optical properties using the Time-Dependent Density Functional Theory (TD-DFT) of the lowest energy neutral, cationic and anionic species to understand how the optical properties are altered by the charge and oxygen content. In Section 2, we outline our theoretical procedures followed. Section 3 describes the changes in the yttrium oxide structure when changing the oxygen content and the charge. We discuss the properties of the neutral and charges species in terms of their thermal stability, ionization potential and electron affinity. We also present the TD-DFT results for the lowest energy geometries of the neutral and charged YO*n* clusters and discuss how the oxygen content changes its optical properties. In Section 4, the conclusion drawn from the above work is presented.

2. Computational details

All the density functional theory calculations were performed with the Gaussian 09 program package [30]. Since the growth motifs of YO*n* clusters are unclear, we have made an extensive search to find the lowest energy structures in two ways (i) by considering the possible structures reported for the first row transition metal oxides and (2) by considering different trial geometries, where oxygen atoms are bound to the yttrium atom molecularly, dissociatively and in the ozonide form [31–34]. All spin multiplicities from singlet to undectet were tried in order to determine the total spin of the ground state, and the default convergence threshold were used during the calculations. The structural optimizations were carried without symmetry constraints using the hybrid B3LYP [35], PBE0 [36] and the pure functional BPW91 [37]. In our previous study, the use of pure functional has provided accurate prediction on the bond parameters, ionization energy and frequencies for the yttrium alloy clusters [38]. In order to induce the scalar relativistic effect for the heavy element yttrium, it was treated with effective core potentials, the Los Alamos set of double-zeta type (Lanl2DZ) basis set [39] and polarized Quadruple-ζ basis set def2-QZVP [40], while the all electron basis set is used for oxygen.

In order to gain insight in to the performance of the different methods, calibration calculations are performed using B3LYP, PBE0 and BPW91 methods with Lanl2DZ and def2-QZVP basis sets. Table 1 provides the bond length, vibrational frequency and vertical electron affinity (VEA) and vertical ionization potentials (VIP) for the neutral and charged YO dimer clusters. All the tested methods predict the ground state geometry, similar to those predicted in the previous works. Furthermore, in all the methods the spin contaminations was found to be low and are close to the theoretical values. The BPW91 method was able to predict vibrational frequencies, VIP, VEA and dissociation energy closer to the experimental values, as compared to the other methods tested. Furthermore, the use of def2-QZVP basis set was essential to predict the stretching frequencies accurately for these clusters. Thus the choice of BPW91/def2-QZVP for DFT calculations is justified as a compromise between reliable results and reasonable computational cost. It should be mentioned that the BPW91 functional has been preferred in the study of transition metal oxides. Since the pure generalized gradient approximation (GGA) functional such as BPW91 usually lead to high symmetry structures, B3LYP calculations are also employed [41]. The first five low lying energy states for all the oxygen compositions were re-optimized using the B3LYP functional with symmetry constraints and the energy discrepancy by different functional was verified. In order to confirm the proper converges to minima, the vibrational frequencies were computed at the BPW91/def2-QZVP level of theory and negative frequency absence was confirmed.

The adiabatic electron affinity (EA_{ad}) is calculated as the energy difference between total energies and the corresponding anion energy at their respective ground state geometries and the adiabatic ionization energy is computed as the energy difference between total energies of a cation and corresponding neutral species at their respective ground state cation energy and corresponding neutral species at their respective ground state spin multiplicity

Table 1
Comparison of geometry, vibrational frequency, vertical ionization potential, vertical electron affinity for yttrium monoxide and yttrium dioxide clusters in their ground states as calculated by B3LYP, BPW91 and PBEPBE functional with Lanl2DZ and Def2-QZVP basis sets.[a]

Cluster	Functional	R_{M-O}, Å	ω, cm^{-1}	VIP, eV	VEA, eV	D_O kcal mol^{-1}
YO	B3LYP	1.837 (1.793)	879.0 (872.5)	6.30 (6.27)	1.33 (1.31)	154 (165)
	BPW91	1.842 (1.797)	861.5 (856.4)	6.13 (6.09)	1.27 (1.31)	169 (174)
	PBEPBE	1.841 (2.775)	861.8 (135.9)	6.18 (6.14)	1.23 (1.27)	172 (181)
Expt		1.790	855.2	5.85 ± 0.15	1.35 ± 0.02	170 ± 2.4
YO^-	B3LYP	1.880 (1.832)	821.2 (813.4)	1.29 (1.26)	3.68 (3.35)	195 (215)
	BPW91	1.882 (1.834)	807.4 (803.9)	1.12 (1.10)	3.56 (3.21)	204 (222)
	PBEPBE	1.882 (1.832)	807.8 (805.0)	1.18 (1.17)	3.56 (3.21)	217 (227)
Expt			740 ± 60			
YO^+	B3LYP	1.799 (1.745)	931.2 (938.8)	15.77 (15.68)	6.35 (6.29)	171 (166)
	BPW91	1.806 (1.752)	909.2 (919.4)	16.02 (15.85)	6.18 (6.13)	189 (185)
	PBEPBE	1.805 (1.751)	910.3 (919.4)	16.05 (15.90)	6.24 (6.17)	192 (188)
Expt			872.0			171.6 ± 6

[a] Values in the parenthesis are from def2-qzvp basis set.

and geometry. The adiabatic ionization energy (AIE) and vertical ionization energies (VIE) are computed as stated in our previous work [38]. The thermodynamic stability of the lowest energy clusters are computed by evaluating different decay channels.

Partial charges analysis was done using the natural bond orbitals program NBO as implemented in Gaussian 09 program at the BPW91/def2-QZVP level of theory [42]. Magnetic moments at the atoms (μ) were calculated following the Mulliken population scheme. The molecular electrostatic potentials (MESP) for all systems were computed using BPW91 functional on the 0.02 a.u. isodensity surface. For the optical part, the calculation on the properties have been carried out in the framework of time dependent-DFT (TDDFT) by extracting a minimum of 300 roots with the time dependent Kohn–Sham formalism by employing BPW91/def2-QZVP level of theory [43]. For comparison, the calculated discrete spectra have been normalized and their peaks broadened with Gaussian function of fwhm = 0.02 eV.

3. Results and discussion

Benchmark calculations of bond length, vertical ionization potential, and electron affinity and bond dissociation energies are performed for the dimer clusters. The computed values along with the available experimental results are summarized in Table 1. The computed bond length R_{M-O} for the neutral dimer at B3LYP/def2-QZVP was 1.797 Å that agrees with the experimental value of 1.790 Å [41]. Further, the predicted vibration frequency, ionization potentials, electron affinity and bond dissociation energies were 856.4 cm^{-1}, 6.09 eV, 1.31 eV and 174 kcal mol^{-1} which are in agreement with the experimental values [44–46]. As evident from Table 1, B3LYP/def2-QZVP has the minimum deviations from the experimental values for charged dimer molecule. The ground state spin multiplicity for neutral dimer was doublet, while that for the charged species was singlet, which agrees well with the previous theoretical works [46]. The R_{M-O} distance for the anion and cation are 1.834 Å and 1.752 Å respectively. The increase and decrease in bond length for anion and cation dimer can be easily understood based on addition or removal of electron from the anti-bonding orbital of neutral dimer cluster.

3.1. Structures of $YOn^{+1/0/-1}$ (n=2–12)

The optimized geometrical configurations along with the spin multiplicity for the lowest energy states of neutral and charged YOn are presented in Fig. 1 (n=2–8) and Fig. 2 (n=9–12). The neutral and anionic geometry of YO_2 cluster exists in oxo form, which is evident from the O–Y–O bond angle of 126.8° and 112.7° respectively. In the cationic form the oxygen atoms bind to the yttrium atom associatively to form peroxide with an O–Y–O bond angle of 67.3°. The bond length of O_2 calculated at BPW91/def2-QZVP was 1.219 Å, which was in close agreement with the experimental value of 1.210 Å [47]. In the cationic YO_2, the peroxide has a bond length of 1.502 Å. This bond enhancement indicates that, during the bonding of O_2, electrons are transfer from oxygen molecule to the yttrium cation. The bond angle and the bond lengths calculated reveal the existence cationic YO_2 in peroxo form. In the trioxides, the oxygen was in oxo and peroxide states in neutral and anion with a ground state multicity of doublet and singlet respectively. The yttrium trioxide anion has oxo and dioxo oxygen atoms. The above results were in good agreement with the previous experimental and theoretical findings [27,46,47]. Recently, Jena and coworkers has found similar ground states geometries for the charged and neutral ScO_3, in which Sc is isoelectronic with yttrium atom [33].

For the tetraoxide, the neutral cluster was found to have a diperoxo structure, while the anion and cation have a dioxo-peroxo structure. The presence of charge on the yttrium atom leads to cleave of the dioxygen molecule. The ground state spin multiplicity for the neutral atom was a doublet, while the anion exists in a triplet ground state. On the other hand the cation was found to have a quintet ground state. Computed results on ScO_4 were found to have a diperoxo structure for the neutral and charge species [33]. For the pentoxide YO_5, the anion and neutral states have one oxo and two peroxo oxygen bound to the yttrium atom; however, the cation state has one ozonide and peroxo oxygen. The geometrical configuration of YO_6 was found to be the same for neutral and charged clusters with oxygen atoms in homoleptic $Y(\eta^2\text{–}O_2)_3$ geometrical configuration. The geometrical configurations of neutral and anionic YOn are similar until n=7, while for the higher n values a drastic difference in geometry was observed. In addition our geometrical configurations obtained for YOn anions are similar to those found previously for the ScOn anions until n=9; however for n=10, 11 and 12 a drastic change in the geometry exists [32].

Due to the presence of odd number of oxygen atoms, for the YO_7 one can expect that the ground state geometry should possess at least one oxo or ozonide form of oxygen. The lowest energy state for the neutral and charged YO_7 species was found to possess a η^2–O_3 ozonide along with a η^2–O_2 diperoxo group; however, the ozonide group has a different orientation. The neutral state was found to be in quartet spin multiplicity, while the charged species were in triplet ground state. The neutral lowest energy state is more stable than the geometrical configuration containing two ozonide species by 0.72 eV. While in the case of anion and cation the geometrical configurations containing two ozonide species were 0.81 eV and 1.21 eV less stable.

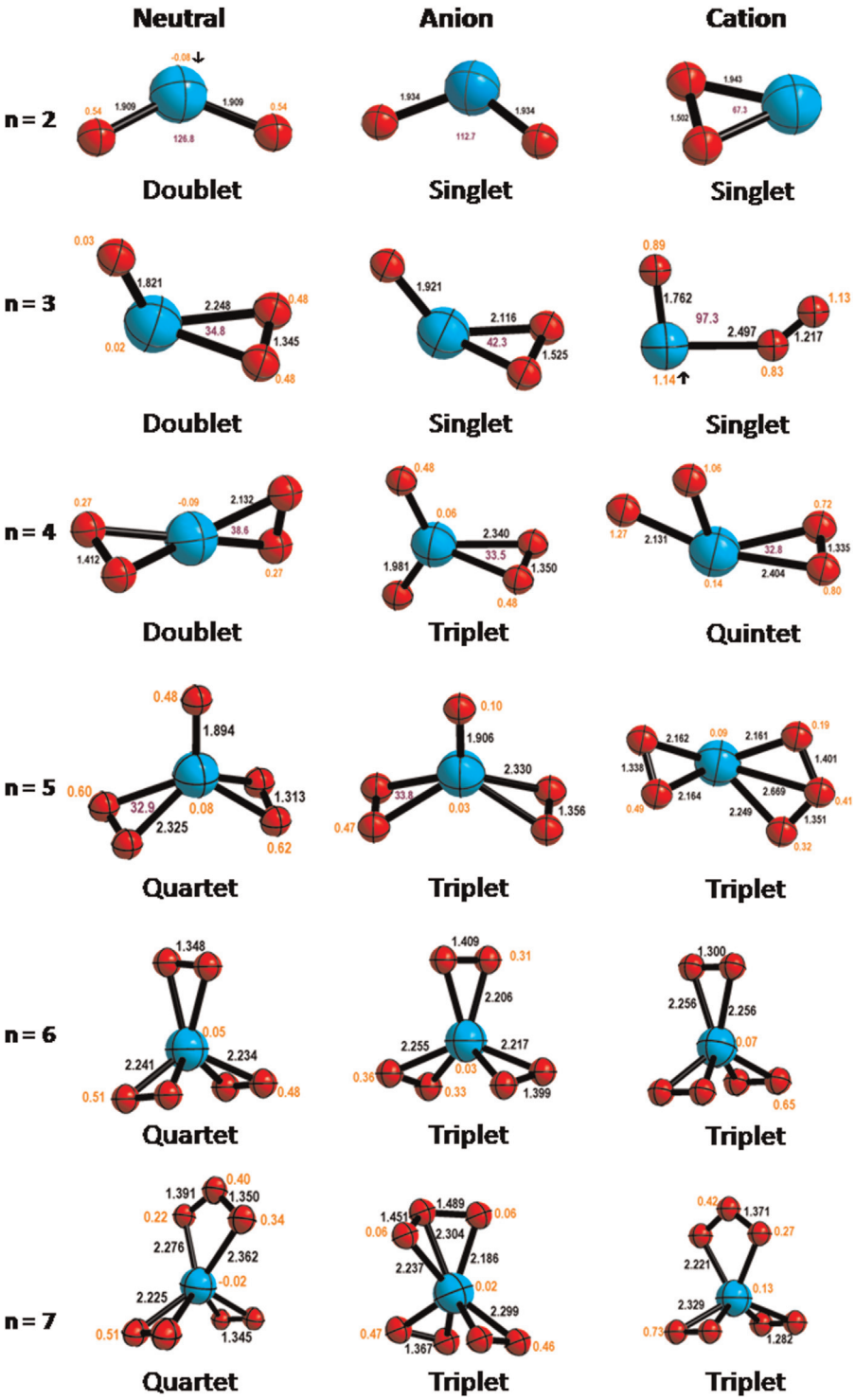

Fig. 1. Geometrical lowest energy state configurations of $YOn^{+1/0/-1}$ (n=2–8) along with important geometrical parameters (bond length in black and bond angle in pink color) and excess spin density (in e) (in yellow color) on the atoms. (For interpretation of the references to color in this figure legend, the reader is referred to the web version of this article.)

The stable geometries for the neutral and charged YO_8 are provided in Fig. 2. The geometrical configuration of YO_8 charged ions was found to be the same with oxygen atoms in homoleptic $Y(\eta^2\text{–}O_2)_4$ geometrical configuration, with the difference in their O_2 orientation. The neutral YO_8 was found to have three peroxo and one end-on superoxo oxygen molecules. In the matrix isolation infrared spectral studies YO_8 was found to exists in a superoxo yttrium bisozonide form, which was 0.73 eV higher in energy than the lowest energy configuration. This difference in the prediction is due to the use of solid matrix in the experimental methods, whereas our DFT predictions are in vaccum [21]. Previously theoretical results on ScO_8 predicted a $Sc(\eta^2\text{–}O_2)_4$ geometrical configuration, while the experimental matrix isolation predicts a $(\eta^2\text{–}O_2)$ Sc $(\eta^2\text{–}O_3)_2$ geometry [32].

The lowest energy YO_9 neutral cluster has sextet spin state with one end-on superoxo, two peroxo and one ozonide form of oxygen. While the anion has a quintet ground state spins multiplicity with three peroxo and one ozonide oxygen. The anion geometrical

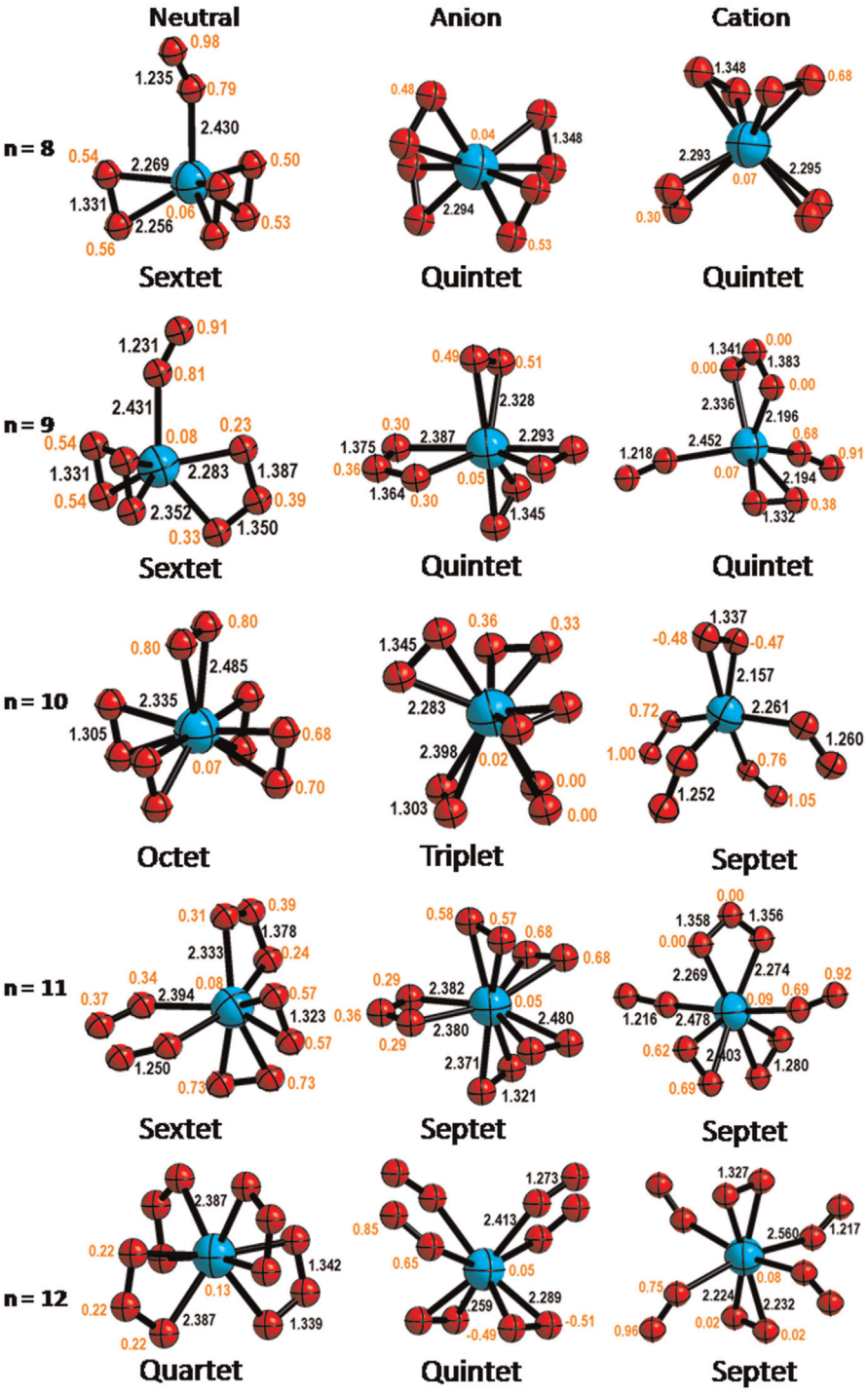

Fig. 2. Geometrical lowest energy state configurations of $YOn^{+1/0/-1}$ (n=9–12) along with important geometrical parameters (bond length in black and bond angle in pink color) and excess spin density (in e) (in yellow color) on the atoms. (For interpretation of the references to color in this figure legend, the reader is referred to the web version of this article.)

configuration of YO_9 resembles that of ScO_9 [32]. The lowest energy cationic YO_9 has a ground spin state of quintet, with two superoxo, one peroxo and one ozonide form of oxygen. For the YO_{10} clusters, there exists several isomers, however, the neutral cluster with the lowest energy state has a penta-peroxo oxygen with a homoleptic $Y(\eta^2\text{–}O_2)_5$ geometrical configuration with the central atom in tenfold coordination. The existence of such tenfold coordination is less surprising as the yttrium resembles lanthanides more than scandium. The anionic form has a similar geometrical configuration; however the oxygen molecules are oriented in a different direction. Contrary to the neutral and anion configurations, the cationic YO_{10} has one peroxo and four superoxo oxygen atoms.

The most stable state of neutral YO_{11} has two peroxo, two superoxo and one ozonide oxygen forms. The cation has eightfold coordination with the same number of peroxo, superoxo and ozonide oxygen, however, the orientation of oxygen atoms is different. The anion has tenfold coordination with four peroxo and one ozonide form of oxygen. It should be pointed out that none of $ScOn$ studied has tenfold coordination [32]. Thus the yttrium atom

resembles lanthanides more than the group three element scandium. It is interesting to observe that the neutral YO_{12} has a tetraozonide form, where the central atom is eightfold coordination. The minimum energy structure of anionic YO_{12} resembles that of ScO_{12} with two peroxo and four superoxo oxygen molecules. The anion has a similar geometrical configuration with peroxo and superoxo groups oriented in different directions.

3.2. Bonding and stability of $YOn^{+1/0/-1}$ ($n=2$–12)

To gain insight on to the nature of bonding in the neutral and charged YO*n* clusters, we have carried out natural bonding analysis, and the results for the various clusters are listed in Table 3 along with the metal atoms charges computed according to the Mulliken population analysis. The charge transfer from the yttrium atom to oxygen ligand is independent of cluster size. In the case of neutral yttrium oxide clusters, the Natural Atomic Orbital (NAO) occupancy charge, (which corresponds to the charge transfer from the metal atom to the ligand) the dimer has 1.91*e*, while in YO_4 the least amount of 1.1*e* charge transfer was observed. On the other hand the Mulliken charge on the central atom remains close to 1.2*e* in most cases. Thus the NAO and Mulliken charges are nearly the same in the neutral YO*n* clusters, while in the anionic series, the small size clusters have small Mulliken charge and higher NAO charge. In the case of cation, clusters beyond $n=6$ have almost the same Mulliken charge, however, for $n=11$ and 12 the NAO charges are much higher than other clusters. This charge difference indicates that bonding in the neutral and charged YO*n* are predominantly ionic in nature.

To analyze the bonding, we have computed the NAO charges for the bare O, O_2, O_3 and YO*n* clusters. The ground state of free standing O_2 was a triplet with effective electronic configuration $2s^{1.81}\ 2p^{4.16}$ while O_3 has $2s^{1.85}\ 2p^{4.25}$ effective electronic configuration for the terminal oxygen and $2s^{1.67}\ 2p^{4.02}$ for the middle oxygen atom. In the neutral dimer YO, the effective electronic configuration on Y was $5s^{0.90}\ 4d^{0.94}\ 5p^{0.11}$ and that on oxygen was $2s^{1.94}\ 2p^{5.13}$. The effective electronic configuration for YO anion, was $5s^{1.80}\ 4d^{0.84}\ 5p^{0.20}$ and on oxygen was $2s^{1.94}\ 2p^{5.23}$, while in cation the configuration was $5s^{0.01}\ 4d^{1.04}\ 5p^{0.04}$ and on oxygen was $2s^{1.95}\ 2p^{4.99}$. Thus there was a transfer of charge from the yttrium atom to the oxygen with major contribution by 5*s* orbital of yttrium atom.

To analyze bonding in peroxo system, we consider the YO_6, which possess three peroxo oxygen molecules with similar geometrical configuration in the neutral and charged states. The net effective electronic configuration of yttrium atom YO_6 in the neutral state is $5s^{0.12}\ 4d^{0.94}\ 5p^{0.21}$, in which $5s^{0.06}\ 4d^{0.43}\ 5p^{0.10}$ electrons contributes for the spin-up and $5s^{0.06}\ 4d^{0.50}\ 5p^{0.11}$ electrons contribute for the spin-down. Thus there exists a spin excess of 0.07*e* on yttrium atom, with main contribution from the 4*d* orbital of yttrium atom. In the oxygen atoms there exists the excess spin of 0.5*e* on each O atom which are antiferromagnetically coupled. Similar phenomena were observed for other charged species. To confirm this further, we have plotted the results on spin densities for the YO_6 neutral and charged species, which are shown in Fig. 3. It is evident from Fig. 3, that excess spins are observed over yttrium atom for the neutral and charged species. Similar result has been observed in the Y_3O_2 and Y_6O_2, where in the total magnetic moments of the clusters are mainly provided by yttrium atoms [26]. To reveal the effect of clusters charge on the bonding, we have computed the NAO charges for the YO_6 neutral and charged clusters which are provided in Table 2. The neutral Y atom on YO_6 has an effective electronic configuration of $5s^{0.12}\ 4d^{0.94}\ 5p^{0.21}$ while the anion and cation has $5s^{0.13}\ 4d^{0.98}\ 5p^{0.23}$ and $5s^{0.11}\ 4d^{0.91}\ 5p^{0.16}$ respectively. The anion with extra electron will occupy the 4*d* orbital of yttrium atom and in cation the 4*d* orbital would remain vacant. However, the observed effective electronic configuration was without considerable change. Thus, the electron addition/removement from the cluster has only modest effect on the bonding, and the entire charge is delocalized over the oxygen ligands.

The molecular electrostatic potential (MESP) topography mapping provides insights into the electrophilic area in clusters. The MESP diagrams for the YO_6 and YO_{11} neutral and charged species are shown in Fig. 4. In both YO_6 and YO_{11} clusters, nucleophilic regions are formed in the vicinity of the oxygen atoms. Upon addition of extra electron, the oxygen atoms were found to have more nucleophilic character than that of the neutral clusters. Thus the added extra electron is distributed over ligands and the central metal atom carries practically the same charge as in the corresponding neutrals, which means that there are stronger electrostatic interactions in the anion species. Upon the removal of electron from neutral cluster, the nucleophilic regions around the oxygen atom got vanished and the whole cluster becomes electrophilic in nature. Thus increased charge delocalization leads to a higher thermodynamic stability with respect to their neutral and cationic yttrium oxides. In order to understand the nature of different oxygen atoms MESP diagram for YO_{11} was plotted which possess oxygen atoms with peroxide and superoxide dioxygen and an ozonide in it. The peroxide-type oxygen's are more strongly nucleophilic than ozonide's which, in turn are more nucleophilic than the superoxides.

To estimate stability of the neutral and charged yttrium oxide complexes towards dissociation, we have computed the energies of decay through the oxygen atom, diatomic oxygen and ozonide channels [14,32]. These energies were obtained as the difference in total energies of the initial and the sum of total energies of the decay fragments including their corresponding zero-point vibration energies' (ZPVE) and are collected in Table 3 for $n=2$–8 and Table 4 for $n=9$–12. For smaller n ($n=2$–9), neutral and anionic YO*n* clusters are thermodynamically stable while for cation clusters with $n=2$–8 were found to be stable. Among the clusters, the anions have higher thermodynamic stability compared to the neutral and cationic clusters. The higher stability of anions can be attributed to the charged delocalization between the metal and the ligand oxygen atoms. Furthermore, among the neutral and

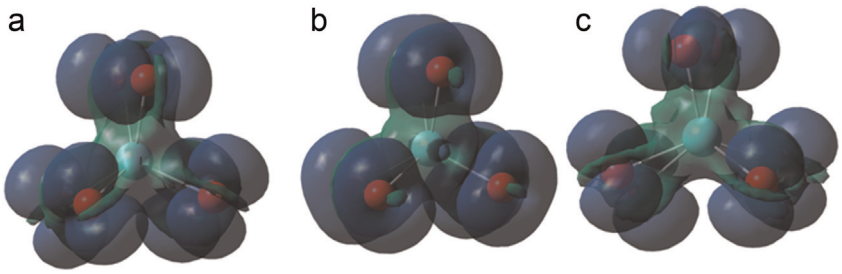

Fig. 3. Spin excess (green color) and depletion (blue color) change density for the neutral and charged YO_6 clusters (a) YO_6 (b) YO_6^- and (c) cation YO_6^+. (For interpretation of the references to color in this figure legend, the reader is referred to the web version of this article.)

Table 2
Natural electron configuration (Ele. Config) (in *e*) and Mulliken charges (q) (in *e*) on the metal atom in neutral and charged state for the YO*n* clusters.

n		Neutral	Anion	Cation	*n*		Neutral	Anion	Cation
1	Ele. Config	$5s^{0.90}\ 4d^{0.90}\ 5p^{0.11}$	$5s^{1.79}\ 4d^{0.80}\ 5p^{0.20}$	$5s^{0.02}\ 4d^{0.99}\ 5p^{0.03}$	7	Ele. Config	$5s^{0.16}\ 4d^{0.89}\ 5p^{0.21}$	$5s^{0.16}\ 4d^{1.01}\ 5p^{0.26}$	$5s^{0.15}\ 4d^{0.82}\ 5p^{0.17}$
	q	0.63	−0.27	1.51		q	1.33	1.27	1.39
2	Ele. Config	$5s^{0.03}\ 4d^{1.15}\ 5p^{0.08}$	$5s^{0.11}\ 4d^{1.29}\ 5p^{0.20}$	$5s^{0.05}\ 4d^{0.91}\ 5p^{0.02}$	8	Ele. Config	$5s^{0.15}\ 4d^{1.07}\ 5p^{0.26}$	$5s^{0.17}\ 4d^{1.11}\ 5p^{0.32}$	$5s^{0.16}\ 4d^{1.02}\ 5p^{0.26}$
	q	1.22	0.63	1.57		q	1.24	1.36	1.33
3	Ele. Config	$5s^{0.05}\ 4d^{1.18}\ 5p^{0.10}$	$5s^{0.07}\ 4d^{1.18}\ 5p^{0.14}$	$5s^{0.66}\ 4d^{0.90}\ 5p^{0.04}$	9	Ele. Config	$5s^{0.17}\ 4d^{1.02}\ 5p^{0.27}$	$5s^{0.19}\ 4d^{1.07}\ 5p^{0.33}$	$5s^{0.15}\ 4d^{0.89}\ 5p^{0.20}$
	q	1.15	0.86	1.19		q	1.24	1.35	1.32
4	Ele. Config	$5s^{0.08}\ 4d^{0.91}\ 5p^{0.11}$	$5s^{0.06}\ 4d^{1.12}\ 5p^{0.20}$	$5s^{0.08}\ 4d^{0.87}\ 5p^{0.08}$	10	Ele. Config	$5s^{0.19}\ 4d^{1.25}\ 5p^{0.39}$	$5s^{0.19}\ 4d^{1.22}\ 5p^{0.39}$	$5s^{0.16}\ 4d^{0.82}\ 5p^{0.22}$
	q	1.25	1.11	1.46		q	1.20	1.28	1.32
5	Ele. Config	$5s^{0.08}\ 4d^{1.08}\ 5p^{0.16}$	$5s^{0.08}\ 4d^{1.12}\ 5p^{0.22}$	$5s^{0.12}\ 4d^{0.74}\ 5p^{0.08}$	11	Ele. Config	$5s^{0.19}\ 4d^{1.08}\ 5p^{0.32}$	$5s^{0.22}\ 4d^{1.26}\ 5p^{0.41}$	$5s^{0.19}\ 4d^{1.03}\ 5p^{0.30}$
	q	1.27	1.09	1.52		q	1.22	1.26	1.24
6	Ele. Config	$5s^{0.12}\ 4d^{0.94}\ 5p^{0.21}$	$5s^{0.13}\ 4d^{0.98}\ 5p^{0.23}$	$5s^{0.11}\ 4d^{0.91}\ 5p^{0.16}$	12	Ele. Config	$5s^{0.27}\ 4d^{0.94}\ 5p^{0.36}$	$5s^{0.19}\ 4d^{1.09}\ 5p^{0.34}$	$5s^{0.17}\ 4d^{1.07}\ 5p^{0.31}$
	q	1.32	1.28	1.38		q	1.28	1.28	1.14

Table 3
Dissociation energies of $YOn^{+1/0/-1}$ n=2–8 through different decay channels.

Channel		E_o(eV)	Channel		E_o(eV)	Channel		E_o(eV)
	Neutral			Anion			Cation	
YO_2 →	YO+O	7.24	YO_2^- →	YO^- + O	7.79	YO_2^+ →	YO^+ + O	5.89
→	Y+O_2	6.26	→	Y^-+O_2	8.62	→	Y^++O_2	5.25
YO_3 →	YO_2+O	4.47	YO_3^- →	YO_2^- + O	6.70	YO_3^+ →	YO_2^+ + O	6.03
→	YO+O_2	0.13	→	YO^-+O_2	2.90	→	YO^++O_2	0.35
YO_4 →	YO_3+O	8.57	YO_4^- →	YO_3^-+O	7.17	YO_4^+ →	YO_3^++O	6.84
→	YO_2+O_2	1.45	→	YO_2^-+O_2	2.29	→	YO_2^++O_2	1.29
→	YO+O_3	4.35	→	YO^-+O_3	5.74	→	YO^++O_3	2.85
YO_5 →	YO_4+O	6.11	YO_5^- →	YO_4^-+O	6.79	YO_5^+ →	YO_4^++O	5.39
→	YO_3+O_2	3.10	→	YO_3^-+O_2	2.39	→	YO_3^++O_2	0.65
→	YO_2+O_3	3.23	→	YO_2^-+O_3	4.75	→	YO_2^++O_3	2.34
→	YO+$2O_2$	3.21	→	YO^-+$2O_2$	5.29	→	YO^++$2O_2$	0.99
YO_6 →	YO_5+O	7.08	YO_6^- →	YO_5^-+O	6.62	YO_6^+ →	YO_5^++O	6.74
→	YO_4+O_2	1.61	→	YO_4^-+O_2	1.84	→	YO_4^++O_2	0.55
→	YO_3+O_3	5.83	→	YO_3^-+O_3	4.67	→	YO_3^++O_3	3.05
→	YO_2+$2O_2$	3.06	→	YO_2^-+$2O_2$	4.13	→	YO_2^++$2O_2$	1.84
YO_7 →	YO_6+O	5.50	YO_7^- →	YO_6^-+O	5.75	YO_7^+ →	YO_6^++O	5.21
→	YO_5+O_2	1.00	→	YO_5^-+O_2	0.79	→	YO_5^++O_2	0.37
→	YO_4+O_3	2.77	→	YO_4^-+O_3	3.25	→	YO_4^++O_3	1.42
→	YO_3+$2O_2$	4.09	→	YO_3^-+$2O_2$	3.18	→	YO_3^++$2O_2$	1.02
→	YO+$3O_2$	4.22	→	YO^-+$3O_2$	6.09	→	YO^++$3O_2$	1.37
YO_8 →	YO_7+O	6.24	YO_8^- →	YO_7^-+O	6.77	YO_8^+ →	YO_7^++O	18.74
→	YO_6+O_2	0.17	→	YO_6^-+O_2	0.95	→	YO_6^++O_2	12.37
→	YO_5+O_3	2.91	→	YO_5^-+O_3	3.23	→	YO_5^++O_3	14.77
→	YO_4+$2O_2$	1.77	→	YO_4^-+$2O_2$	2.78	→	YO_4^++$2O_2$	12.92
→	YO_2+$2O_3$	6.13	→	YO_2^-+$2O_3$	7.98	→	YO_2^++$2O_3$	17.12

charged YO_8 clusters, YO_8^+ have higher thermodynamic stability, which can be attributed to the octa coordination of oxygen atoms. It is evident from the Table 4, YO_{10}^+ and YO_{12}^+ are highly exothermic to the release of one and two oxygen molecules with the formation of YO_8^+ species. In addition, the ozone dissociation channel, for YO_{11}^+ was also exothermic and was 1.42 eV less energetic as compared to O_2 dissociation channel. Thus, by changing the charges, it is possible to release the oxygen from the YO*n* clusters. In addition, the dissociation values are much higher than these in the isoelectronic ScO*n*, indicating their ability to act as oxygen reducing agent for metals.

The computed vertical and adiabatic electron affinity, vertical and adiabatic ionization potential for the neutral clusters are presented in Table 5. The vertical and adiabatic EAs and IPs provides information about the relative stability of the neutral and ionic clusters. The IP and EAs values for the YO cluster are 1.35 eV and 5.85 eV obtained by photoionization spectrum [19]. Our computed values are 1.31 eV and 6.09 eV which are in close agreement with them. Wu and coworkers have provided values of 1.36 and 6.418 while using the B3LYP with SDD basis set [46]. The vertical and adiabatic electron affinities of the clusters increase monotonically with the increase in cluster size except the YO_3, whose value is much higher compared to other small size cluster. On the other hand, the computed the adiabatic and vertical ionization potential of the clusters, show an oscillator behavior with the increasing *n*. The VIP and AIP values for YO_3, and YO_8 were found to less compare to other clusters studied. The low ionization value and high electron affinity of YO_3 indicates its higher stability. The computed highest occupied molecular orbital-lowest unoccupied molecular orbital (HOMO–LUMO) gap for the neutral cluster are provided in Table 5. The HOMO–LUMO gap of the clusters decreases

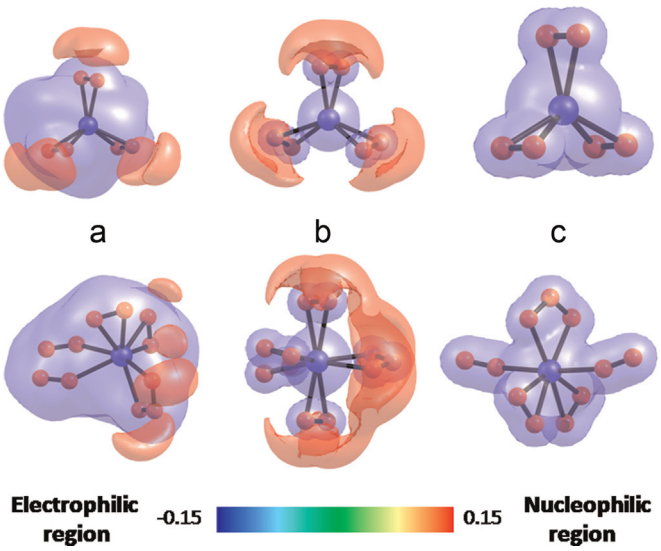

Fig. 4. Selection of representative 3D Molecular Electrostatic Potential (MEPs) mapped on an electron density surface of 0.02 a.u. for neutral and charged YO_6 and YO_{11} clusters. (a) neutral (b) anionic and (c) cationic clusters.

monotonically with the increase in cluster size. This is due to the increase in the number of *s* and *p* orbitals of oxygen atom which increases in cluster size.

3.3. Optical properties of YOn, YOn^+ and YOn^- (n=2–12)

The calculated optical absorption spectra for the yttrium oxide anion cluster with $n=1$–5 and $n=7$–12 are shown in Figs. 5 (a) and (b). We are unable to calculate the absorption spectra for the YO_6^- cluster, due to the excess mixing of valence and core orbitals. Fig. 6(a) shows the absorption spectra for YO_8 neutral and charged clusters. The respective HOMO and LUMO orbital's for the neutral and charged YO_8 are provided in Fig. 6(b). Our simulated absorption spectral patterns for YO to YO_5 anions are in close agreement with the previous experimental result with a slight difference in the area of maximum absorption [46]. Such differences in the energy between the DFT and experimental results have been previously observed for various metal oxide clusters [48].

The main adsorption peaks for yttrium oxide clusters occur in range from 1.1 to 2.5 eV, 4.5 to 8.2 eV. The absorption spectra of YO shows several peaks which are mainly contributed by yttrium metal *d* and oxygen *s* and *p* valence orbitals, which is evident from the HOMO and LUMO diagrams. Furthermore, with the increase in cluster size the number of *s* and *p* orbital population of oxygen atom increases. Thus the absorption peaks are mainly contributed by oxygen atoms *s* and *p* orbitals in larger clusters. From the calculated spectra, we can see a shifting tendency of the absorbance bands towards lower energy with the increase in the number of oxygen atoms in the clusters. The transitions of low energy shift in anion clusters are due to the excitations from the *p* orbitals, to the

Table 5
Computed adiabatic electron affinities (AEA), vertical electron affinities (VEA), adiabatic ionization potentials (AIP), vertical ionization potentials (VIP) and HOMO–LUMO band gap (E_{gap}) for the neutral yttrium oxide clusters YO*n* ($n=1$–12).

n	AEA	VEA	AIP	VIP	E_{gap} (eV)
1	1.12	1.31	6.00	6.27	1.29
2	1.68	1.63	7.19	6.24	1.01
3	3.91	3.40	5.54	1.31	1.11
4	2.52	2.06	7.08	3.03	0.33
5	3.20	3.29	7.65	6.17	0.55
6	2.75	2.89	7.91	5.53	0.77
7	3.00	2.94	8.06	5.79	0.63
8	3.53	3.44	4.53	3.39	0.40
9	3.72	3.65	7.67	8.49	0.65
10	3.61	3.93	7.42	8.13	0.54
11	3.88	4.18	7.03	8.72	0.46
12	5.27	4.67	5.28	8.51	0.20

Table 4
Dissociation energies of $YOn^{+1/0/-1}$ $n=9$–12 through different decay channels.

Channel		E_o(eV)	Channel		E_o(eV)	Channel		E_o(eV)
	Neutral			**Anion**			**Cation**	
YO_9 →	YO_8+O	5.42	YO_9^- →	YO_8^-+O	5.61	YO_9^+ →	YO_8^++O	**−6.90**
→	YO_7+O_2	0.08	→	$YO_7^-+O_2$	0.81	→	$YO_7^++O_2$	0.26
→	YO_6+O_3	1.25	→	$YO_6^-+O_3$	2.16	→	$YO_6^++O_3$	1.13
→	YO_5+2O_2	1.09	→	$YO_5^-+2O_2$	1.60	→	$YO_5^++2O_2$	0.63
→	YO_3+3O_2	4.18	→	$YO_3^-+3O_2$	3.98	→	$YO_3^++3O_2$	1.28
→	$YO+4O_2$	4.30	→	YO^-+4O_2	6.89	→	YO^++4O_2	1.62
→	YO_3+2O_3	7.09	→	$YO_3^-+2O_3$	6.89	→	$YO_3^++2O_3$	4.19
YO_{10} →	YO_9+O	6.01	YO_{10}^- →	YO_9^-+O	5.90	YO_{10}^+ →	YO_9^++O	6.05
→	YO_8+O_2	**−0.15**	→	$YO_8^-+O_2$	**−0.07**	→	$YO_8^++O_2$	**−12.43**
→	YO_7+O_3	1.75	→	$YO_7^-+O_3$	2.37	→	$YO_7^++O_3$	1.97
→	YO_6+2O_2	0.01	→	$YO_6^-+2O_2$	0.88	→	$YO_6^++2O_2$	**−0.06**
→	YO_4+3O_2	1.62	→	$YO_4^-+3O_2$	2.72	→	$YO_4^++3O_2$	0.49
→	YO_2+4O_2	3.08	→	$YO_2^-+4O_2$	5.01	→	$YO_2^++4O_2$	1.77
→	YO_4+2O_3	4.53	→	$YO_4^-+2O_3$	5.63	→	$YO_4^++2O_3$	3.39
YO_{11} →	$YO_{10}+O$	5.32	YO_{11}^- →	YO_{10}^-+O	5.58	YO_{11}^+ →	YO_{10}^++O	5.67
→	YO_9+O_2	**−0.25**	→	$YO_9^-+O_2$	**−0.09**	→	$YO_9^++O_2$	0.13
→	YO_8+O_3	0.83	→	$YO_8^-+O_3$	1.17	→	$YO_8^++O_3$	**−11.01**
→	YO_7+2O_2	**−0.17**	→	$YO_7^-+2O_2$	0.71	→	$YO_7^++2O_2$	0.39
→	YO_5+3O_2	0.83	→	$YO_5^-+3O_2$	1.51	→	$YO_5^++3O_2$	0.77
→	YO_3+4O_2	3.93	→	$YO_3^-+4O_2$	3.89	→	$YO_3^++4O_2$	1.41
YO_{12} →	$YO_{11}+O$	4.60	YO_{12}^- →	YO_{11}^-+O	5.99	YO_{12}^+ →	YO_{11}^++O	6.23
→	$YO_{10}+O_2$	**−1.66**	→	$YO_{10}^-+O_2$	**−0.01**	→	$YO_{10}^++O_2$	0.32
→	YO_9+O_3	0.01	→	$YO_9^-+O_3$	1.56	→	$YO_9^++O_3$	2.03
→	YO_8+2O_2	**−1.81**	→	$YO_8^-+2O_2$	**−0.07**	→	$YO_8^++2O_2$	**−12.11**
→	YO_6+3O_2	**−1.64**	→	$YO_6^-+3O_2$	0.87	→	$YO_6^++3O_2$	0.26

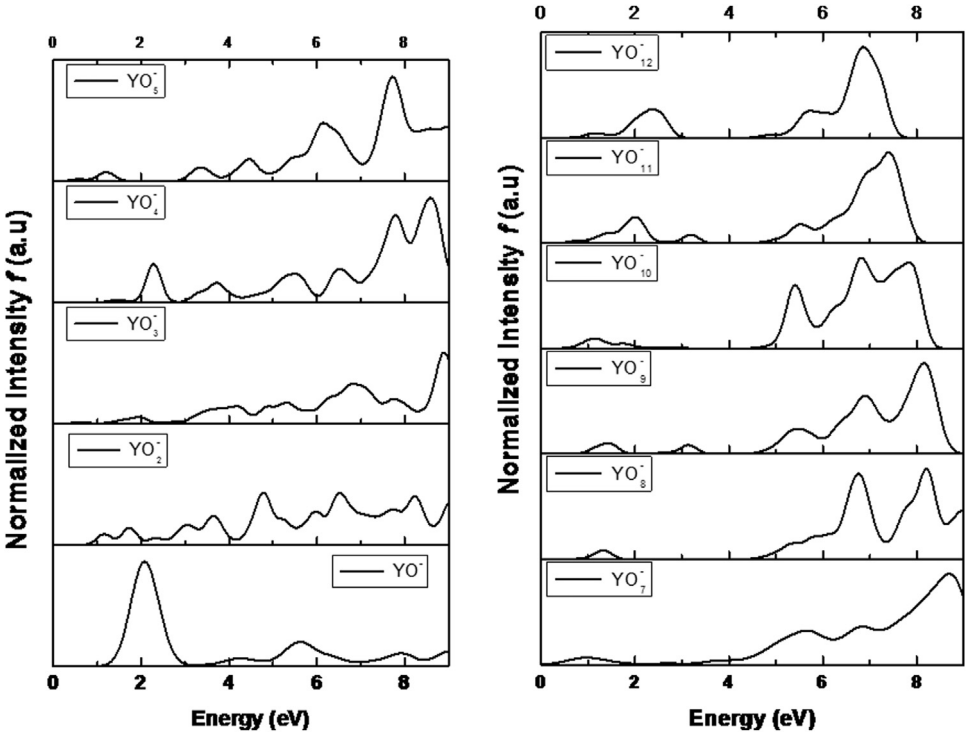

Fig. 5. TD-DFT calculations of the optical absorption spectra for anionic YOn (n=1–5) clusters.

region with an $s+p$ character of oxygen atoms. Thus the increase in oxygen content results in low energy transition which are mainly contributed by the oxygen 2p orbitals. To understand the effect of charge on the optical properties we have plotted the absorption spectra for the neutral and charged YO_8 clusters. From the spectra it is obvious that the absorption peak positions are not affected by the effect of charge, however, there exists a splitting in the peaks, which are due to the different orbital excitations.

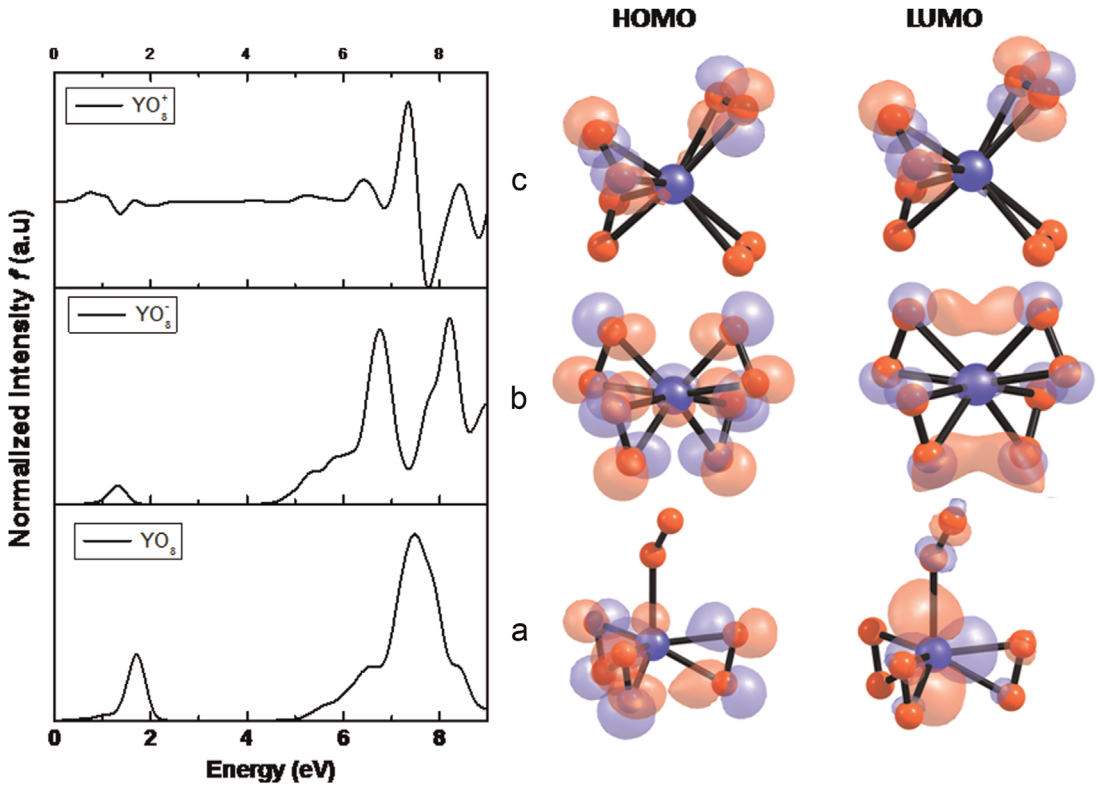

Fig. 6. TD-DFT calculations of the optical absorption spectra for anionic YOn (n=7–12) clusters.

4. Conclusion

We report a systematic study on the structure, stability and optical properties of neutral and charged YO*n* clusters. Small size clusters with $n < 7$ resemble the isoelectronic scandium oxide clusters. In large clusters a drastic difference in geometrical configuration was observed. The oxygen atom in YO*n* were in oxo, peroxo and in superoxo forms. We found YO_{10} cluster to have a penta-peroxo oxygen with a homoleptic $Y(\eta^2\text{–}O_2)_5$ geometrical configuration, making yttrium behavior to be similar to that of lanthanides with higher coordination sites. The geometrical structures and topologies of anions and neutral are similar, although there are some differences in the large cluster. The NAO charge on Y atom varies slightly both with the number of oxygen atom and on charges, which indicates the electron is entirely delocalized over oxygen atoms. Further, HOMO–LUMO gaps decrease with increasing *n* due to the increase in 2*p* orbital population of oxygen atom. The MESP diagram indicates that the peroxide type atoms are more strongly nucleophilic than ozonide and superoxide oxygen's.

The bonding in these clusters are predominantly ionic in nature. Among the clusters, anions have higher thermodynamic stability as compared to that of the neutral and cations, due to the effective charge delocalization between the metal atom and oxygen ligands. YO_{10}^{+} and YO_{12}^{+} were found to be highly exothermic to release one and two oxygen atoms, while YO_{11}^{+} dissociates though ozonide dissociation channel. The main absorption peak for the clusters occurs in the range from 1.1 to 2.5 eV and 4.5 to 8.2 eV. The absorption spectra of small clusters are mainly contributed by yttrium metal *d* and *s* valence orbitals. The shift of absorbance towards lower energy was observed with the increase of the oxygen content, while the charge has little effect on the absorption spectrum.

Acknowledgments

The author thanks the SASTRA University for the constant encouragement and for providing necessary infrastructure. The author thanks the DST for funding through a project (No. SB/S1/PC-047/2013). The author thanks the crew of the Center for Computational Materials Science at Institute for Materials Research, Tohoku University, for their continuous support of the HITACHI SR16000 supercomputing facility.

References

[1] C.N.R. Rao, B. Raveau, Transition Metal Oxides: Structure, Properties and Synthesis of Ceramic Oxides, Wiley-VCH, New York/Weinheim, 1998.
[2] K.A. Zemski, D.R. Justes, A.W. Castleman, J. Phys. Chem. B 106 (2002) 6136.
[3] H.-J. Zhai, J. Döbler, J. Sauer, l-S. Wang, J. Am. Chem. Soc 129 (2007) 13270.
[4] G.L. Gutsev, C.A. Weatherford, K. Pradhan, P. Jena, J. Phys. Chem. A 114 (2010) 9014.
[5] Y. Gong, M. Zhou, Phys. Chem. Chem. Phys. 11 (2009) 8714.
[6] H.-J. Zhai, W.-J. Chen, S.-J. Lin, X. Huang, l-S. Wang, J. Phys. Chem. A 117 (2013) 1042.
[7] C.R. Varney, D.T. Mackay, S.M. Reda, F.A. Selim, J. Phys. D: Appl. Phys. 45 (2012) 015103.
[8] E.J. Rubio, V.V. Atuchin, V.N. Kruchinin, L.D. Pokrovsky, C.V. Ramana, J. Phys. Chem. C 118 (2014) 13644.
[9] J.R. Jayaramaiah, B.N. Lakshminarasappa, B.M. Nagabhushana, Sens. Actuators B: Chem. 173 (2012) 234.
[10] A. Fukabori, T. Yanagida, J. Pechal, S. Maeo, Y. Yokota, A. Yoshikawa, T. Ikegami, F. Moretti, K. Kamada, J. Appl. Phys. 107 (2001) 073501.
[11] V.H. Mudavakkat, V.V. Atuchin, V.N. Kruchinin, A. Kayani, C.V. Ramana, Opt. Mater. 34 (2012) 893.
[12] M. Mishra, P. Kuppusami, T.N. Sairam, A. Singh, E. Mohandas, Appl. Surf. Sci. 257 (2011) 7665.
[13] C.V. Ramana, V.H. Mudavakkat, K.K. Bharathi, V.V. Atuchin, L.D. Pokrovsky, V. N. Kruchinin, App. Phys. Lett. 98 (2011) 031905.
[14] Y. Gong, M. Zhou, L. Andrews, Chem. Rev. 109 (2009) 6765.
[15] l-H. Tian, Y.-X. Zhao, X.-N. Wu, X.-L. Ding, S.-G. He, T.-M. Ma, ChemPhysChem 13 (2012) 1282.
[16] J. Yuan, H.-G. Xu, X. Kong, W. Zheng, Chem. Phys. Lett. 564 (2013) 6.
[17] K. Pradhan, G.L. Gutsev, C.A. Weatherford, P. Jena, J. Chem. Phys. 134 (2011) 144305.
[18] E.L. Uzunova, J. Phys. Chem. A 115 (2011) 1320.
[19] M.B. Knickelbein, J. Chem. Phys. 102 (1995) 1.
[20] Y. Zhao, Y. Gong, M. Chen, C. Ding, M. Zhou, J. Phys. Chem. A 109 (2005) 11765.
[21] Y. Gong, G. Ding, M. Zhou, J. Phys. Chem. A 113 (2009) 8509.
[22] L. Andrews, M. Zhou, G.V. Chertihin, C.W. Bauschlicher Jr, J. Phys. Chem. A 103 (1999) 6525.
[23] A. Pramann, Y. Kakamura, A. Nakajima, K. Kaya, J. Phys. Chem. A 105 (2001) 7534.
[24] Z.D. Reed, M.A. Duncan, J. Phys. Chem. A 112 (2008) 5354.
[25] Z. Yang, S.-J. Xiong, J. Chem. Phys. 129 (2008) 124308.
[26] Z. Yang, S.-J. Xiong, J. Phys. Chem. A 114 (2010) 54.
[27] E.P.F. Lee, J.M. Dyke, D.K.W. Mok, F.-t Chau, J. Phys. Chem. A 112 (2008) 4511.
[28] Z. Yang, S.-J. Xiong, J.Phys. B: At. Mol. Opt. Phys. 42 (2009) 245101.
[29] A.B. Rahane, P.A. Murkute, M.D. Deshpande, V. Kumar, J. Phys. Chem. A 117 (2013) 5542.
[30] M. J. Frisch, G. W. Trucks, H. B. Schlegel, G. E. Scuseria, M. A. Robb, J. R. Cheeseman, G. Scalmani, V. Barone, B. Mennucci, G. A. Petersson, H. Nakatsuji, M. Caricato, X. Li, H. P. Hratchian, A. F. Izmaylov, J. Bloino, G. Zheng, J. L. Sonnenberg, M. Hada, M. Ehara, K. Toyota, R. Fukuda, J. Hasegawa, M. Ishida, T. Nakajima, Y. Honda, O. Kitao, H. Nakai, T. Vreven, J. A. Montgomery, Jr., J. E. Peralta, F. Ogliaro, M. Bearpark, J. J. Heyd, E. Brothers, K. N. Kudin, V. N. Staroverov, T. Keith, R. Kobayashi, J. Normand, K. Raghavachari, A. Rendell, J. C. Burant, S. S. Iyengar, J. Tomasi, M. Cossi, N. Rega, J. M. Millam, M. Klene, J. E. Knox, J. B. Cross, V. Bakken, C. Adamo, J. Jaramillo, R. Gomperts, R. E. Stratmann, O. Yazyev, A. J. Austin, R. Cammi, C. Pomelli, J. W. Ochterski, R. L. Martin, K. Morokuma, V. G. Zakrzewski, G. A. Voth, P. Salvador, J. J. Dannenberg, S. Dapprich, A. D. Daniels, O. Farkas, J. B. Foresman, J. V. Ortiz, J. Cioslowski, and D. J. Fox, Gaussian G09, Revision C.01, Gaussian, Inc., Wallingford CT, 2010.
[31] G.L. Gutsev, G.W. Bauschlicher Jr., H.-J., Zhai, l-S., Wang, J. Chem. Phys. 119 (2003) 11135.
[32] G.L. Gutsev, C.A. Weatherford, K. Pradhan, P. Jena, J. Comput. Chem. 32 (2011) 2974.
[33] K. Pradhan, G.L. Gutsev, C.A. Weatherford, P. Jena, J. Chem. Phys. 134 (2011) 144305.
[34] S. Li, D.A. Dixon, J. Phys. Chem. A. 111 (2007) 11908.
[35] (a) P.J. Stephens, F.J. Devlin, C.F. Chabalowski, M.J. Frisch, J. Phys. Chem. 98 (1994) 11623;
(b) A.D. Becke, J. Chem. Phys. 98 (1993) 5648.
[36] C. Adamo, V. Barone, J. Chem. Phys. 110 (1999) 6158.
[37] (a) J.P. Perdew, Y. Wang, Phys. Rev. B 45 (1992) 13244;
(b) A.D. Becke, Phys. Rev. A 38 (1988) 3098.
[38] N.S. Venkataramanan, A. Suvitha, R. Note, Y. Kawazoe, J. Mol. Struct.: Theochem. 902 (2009) 72.
[39] W.R. Wadt, P.J. Hay, J. Chem. Phys. 82 (1985) 270.
[40] F. Weigend, Phys. Chem. Chem. Phys. 8 (2006) 1057.
[41] G.L. Gutsev, C.A. Weatherford, K. Pradhan, P. Jena, J. Phys. Chem. A 114 (2010) 9014.
[42] J.P. Foster, F. Weinhold, J. Am. Chem. Soc. 102 (1980) 7211.
[43] P. Hohenberg, W. Kohn, Phys. Rev. 136 (1964) B864.
[44] K.-P. Huber, G. Herzberg, Molecular spectra and molecular structures, in: K.-P. Huber, G. Herzberg (Eds.), Constants of Diatomic Molecules, vol. IV, Van Nostrand, Reinhold Company, New York, 1979.
[45] S.G. Lias, J.E. Bartmes, J.F. Liebman, J.L. Holmes, R.D. Levin, W.G. Mallard, J. Phys. Chem. Ref. Data 17 (1) (1988).
[46] H. Wu, l-S. Wang, J. Phys. Chem. A 102 (1998) 9129.
[47] K.M. Ervin, I. Anusiewicz, P. Skurski, J. Simsons, W.C. Lineberger, J. Phys. Chem. A 107 (2003) 8521.
[48] H.-J. Zhai, W.-J. Chen, S.-J. Lin, X. Huang, l-S. Wang, J. Phys. Chem. A 117 (2013) 1042.